*J. Fluid Mech.* (2002), *vol.* 459, *pp.* 93–102.  
DOI: 10.1017/S0022112002008169 Printed in the United Kingdom

# Relationship between the intrinsic radial distribution function for an isotropic field of particles and lower-dimensional measurements

By GRETCHEN L. HOLTZER AND LANCE R. COLLINS†

Department of Chemical Engineering, The Pennsylvania State University, University Park, PA 16802, USA

(Received 20 December 2001 and in revised form 2 February 2002)

In this paper, we present relationships between the intrinsic radial distribution function (RDF) for a three-dimensional, isotropic system of particles and the lower-dimensional RDFs obtained experimentally from either two-dimensional or one-dimensional sampling of the data. The lower-dimensional RDFs are shown to be equivalent to integrals of the three-dimensional function, and as such contain less information than their three-dimensional counterpart. An important consequence is that the lower-dimensional RDFs are attenuated at separation distances below the characteristic length scale of the measurement. In addition, the inverse problem (calculating the three-dimensional RDF from the lower-dimensional measurements) is not well posed. However, recent results from direct numerical simulations (Reade & Collins 2000) showed that the three-dimensional RDF for aerosol particles in a turbulent flow field obeys a power-law dependence on $r$ for $r \ll \eta$, where $\eta$ is the Kolmogorov scale of the turbulence. In this case, the inverse problem is well posed and it is possible to obtain the prefactor and exponent of the power law from one- or two-dimensional measurements. A procedure for inverting the data is given. All of the relationships derived in this paper have been validated by data derived from direct numerical simulations.

## 1. Introduction

Heavy particles in a turbulent flow field tend to cluster in high-strain regions of the flow due to a 'centrifuge' effect of the vorticity (Squires & Eaton 1991; Wang & Maxey 1993). This clustering can lead to superconcentrations of particles that are orders of magnitude greater than the average concentration of particles. Sundaram & Collins (1997) showed that particle clustering modifies the collision kernel by a factor equal to the radial distribution function (RDF) evaluated at particle contact. Recent numerical studies of turbulent coagulation of finite-inertia particles have focused on measuring the RDF (Reade & Collins 2000*a*, *b*; Wang, Wexler & Zhou 2000).

Experimental measurement of the RDF of solid particles at low Reynolds numbers has recently been accomplished (Lei, Ackerson & Tong 2001); however, equivalent measurements in a turbulent flow field have yet to be made. An important complication with turbulent flow experiments is that the characteristic length of the clusters

† Author to whom correspondence should be addressed. Current address: Mechanical and Aerospace Engineering, Cornell University, Ithaca, NY 14853–7501, USA.

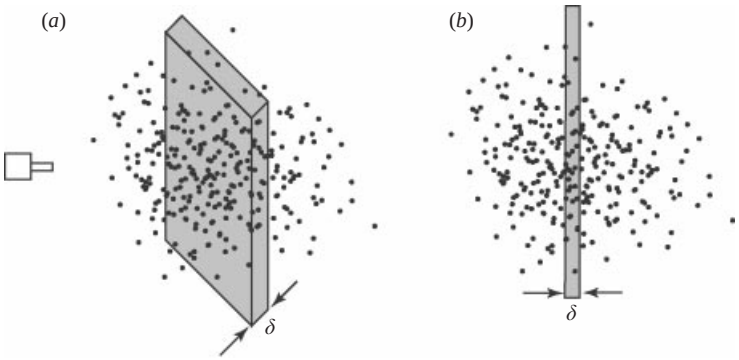


FIGURE 1. Schematic of (*a*) a two-dimensional laser sheet of thickness $\delta$ going through a three-dimensional particle field, and (*b*) a one-dimensional sampling of the same particles using a probe of cross-section $\delta^2$.

is small, scaling with the Kolmogorov length of the turbulence $\eta = (\nu^3/\epsilon)^{1/4}$, where $\nu$ is the kinematic viscosity of the fluid and $\epsilon$ is the turbulent energy dissipation rate per unit mass. This dimension can be fractions of a millimetre or smaller in gas flows (including atmospheric conditions) making the imaging of these clusters a challenge. A second complication is that three-dimensional particle imaging is both technically challenging and costly, and therefore is not widely available (see for example Zhang, Tao & Katz 1997; Pu & Meng 2000). Consequently, particle positions are often obtained from lower-dimensional sampling of the system. Figure 1 shows two examples. In the first experiment, a laser sheet of thickness $\delta$ is used to illuminate a two-dimensional slice through the particle field. A charged coupled device (CCD) camera oriented perpendicularly to the incident light can then record the $(x, y)$ positions of the particles that are illuminated. A second approach, shown schematically in figure 1(*b*), is to sample particle positions along a linear trajectory through the particle field with a probe of cross-section defined as $\delta^2$. An important example of this is the forward scatter spectrometer probe (FSSP) used by cloud physicists to measure distributions of cloud droplets (Baker 1992). A higher-speed version of the probe (Fast FSSP) has lead to more refined measurements and analysis (Brenguier *et al.* 1998; Kostinski & Shaw 2001).

We will show that one- or two-dimensional sampling of the data (even in the absence of experimental error) yields a distribution function that is fundamentally different than the three-dimensional distribution function. Moreover, the discrepancy is especially pronounced at small separations, which is the range of greatest significance to collision processes (Reade & Collins 2000*a*; Wang *et al.* 2000). In § 2 of this paper, we derive the forward relationships between the intrinsic three-dimensional RDF (referred to as $g_{3D}(r)$) and the RDF obtained by sampling the particle field with either a two-dimensional laser sheet ($g_{2D}(r)$) or a one-dimensional sampling probe ($g_{1D}(r)$). The second part of the paper (§ 3) describes ways to make the inverse problem (i.e. calculating $g_{3D}(r)$ from either $g_{2D}(r)$ or $g_{1D}(r)$) well posed and shows how to regress lower-dimensional measurements to obtain $g_{3D}(r)$ for the specific case of a turbulent aerosol.

## 2. Forward relationships

The three-dimensional radial distribution function for a statistically isotropic system of identical particles is defined as the ratio of the number of particle pairs found at

a given separation distance to the expected number if the particles were uniformly distributed (here 'uniformly distributed' means the probability of finding a given particle at a location in space is independent of the positions of the other particles; see McQuarrie 1976). Given the three-dimensional positions of $N$ identical particles, this quantity can be calculated by binning all of the particle pairs according to their separation distances and calculating

$$g_{3D}(r_i) = \frac{P_i/V_i}{P/V}, \tag{2.1}$$

where $P \equiv N(N-1)/2$ is the total number of particle pairs, $P_i$ is the number of pairs with separation distances between $r_i - \Delta r/2$ and $r_i + \Delta r/2$, $V$ is the total volume of the system and $V_i \equiv \frac{4}{3}\pi[(r_i + \Delta r/2)^3 - (r_i - \Delta r/2)^3]$ is the volume of the shell associated with the nominal separation distance $r_i$.

As noted above, measuring the three-dimensional position of particles in a volume involves technology that is still under development. In the meantime, experiments can be done by imaging a two-dimensional plane of particles (see figure 1(*a*)). The resulting $(x, y)$ data can be binned according to particle separation distances, yielding a two-dimensional RDF defined as

$$g_{2D}(r_i) \equiv \frac{\tilde{P}_i/A_i}{\tilde{P}/A}, \tag{2.2}$$

where $\tilde{P}$ is the total number of particle pairs in the slice, $\tilde{P}_i$ is the number of pairs with separation distances between $r_i - \Delta r/2$ and $r_i + \Delta r/2$, $A$ is the total area of the slice and $A_i \equiv \pi[(r_i + \Delta r/2)^2 - (r_i - \Delta r/2)^2]$ is the area of the shell associated with the nominal separation distance $r_i$. Likewise, data obtained by sampling particle positions along a linear path through the particle field can be binned according to separation distance, yielding a one-dimensional RDF defined as

$$g_{1D}(r_i) \equiv \frac{\hat{P}_i/L_i}{\hat{P}/L}, \tag{2.3}$$

where $\hat{P}$ is the total number of particle pairs in a particular sweep, $\hat{P}_i$ is the number of pairs with separation distances between $r_i - \Delta r/2$ and $r_i + \Delta r/2$, $L$ is the total length of the sample, and $L_i \equiv \Delta r$ is the length of the shell.

Figure 2(*a*) shows typical results for $g_{3D}(r)$, $g_{2D}(r)$ and $g_{1D}(r)$ taken from a single realization of a direct numerical simulation (DNS) of finite-inertia particles that neglected gravititational settling (see Reade & Collins 2000*a* for details). The two-dimensional function, $g_{2D}(r)$, was calculated by cutting the DNS volume into 256 slices of equal thickness and computing the RDF according to (2.2), while the one-dimensional function was calculated by cutting the same DNS volume into $256^2$ columns and computing the RDF according to (2.3). Notice that the lower-dimensional RDFs show attenuation at small separations. The dependence of $g_{2D}(r)$ on the size of the slices is shown in figure 2(*b*). The degree of attenuation increases with increasing slice thickness.

### 2.1. *Two-dimensional relationship*

To derive a relationship between $g_{3D}(r/\eta)$ and $g_{2D}(r/\eta)$, we must consider the information that is lost in compressing the three-dimensional data into two dimensions. If we imagine an axis centred on a given test particle within the slice, then the particles that will be counted as lying within the cross-sectional area $A_i$ actually lie within

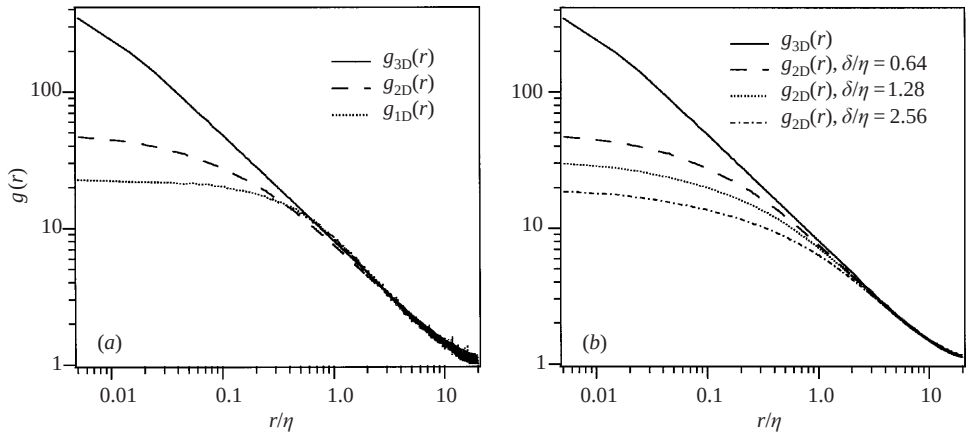


FIGURE 2. (*a*) Comparison of the three-dimensional, two-dimensional and one-dimensional RDF obtained from a single realization of a DNS with $\delta/\eta = 0.64$. (*b*) three-dimensional and two-dimensional RDFs for several $\delta/\eta$, as indicated.

the control volume depicted in figure 3(*a*). Notice that this control volume is not the spherical shell volume denoted by $V_i$, but rather an annular volume defined as $\tilde{V}_i \equiv A_i\delta$. Furthermore, the true separation distance between the test particle and particles lying within this volume will vary by more than just $\Delta r$. Consequently, the expected number of particle pairs must be obtained by integrating $g_{3D}(r)$ over the volume (McQuarrie 1976)

$$\tilde{P}_i = \frac{P}{V}\int_0^{\delta}\int_{r_i-\Delta r/2}^{r_i+\Delta r/2} g_{3D}(\sqrt{r^2+(z-z_0)^2})\,2\pi r\,\mathrm{d}r\,\mathrm{d}z,$$

where the centre of the test particle is defined as $(0, 0, z_0)$. Ideally one would like to have $\delta/\eta \ll 1$. However, laser optics and sampling requirements limit the laser sheet thickness to $\delta \approx 1$ mm (with $\approx 3\%$ variation across the measurement volume, H. Meng 2002, private communication), and the Fast FSSP to approximately 0.1 mm (Chaumat & Brenguier 2001), implying $0.1 < \delta/\eta < 10$, where the low end corresponds to the Fast FSSP and the high end to the two-dimensional laser measurement. It is desirable to obtain the RDF down to near particle contact for accurate prediction of the turbulent collision rate (Wang *et al.* 2000). In many applications where clustering is important (e.g. clouds), the particle diameter is much smaller than the Kolmogorov scale, implying $\Delta r/\eta \ll 1$ (often below $10^{-2}$). Experimentally this poses no problem since $\Delta r$ can be made arbitrarily small (assuming a sufficient sample size); however, this does imply that $\Delta r/\delta \ll 1$ in most applications, which has important consequences for the analysis of the data. Under this circumstance, we can evaluate the radial integral approximately, yielding

$$\tilde{P}_i \approx \frac{P A_i}{V}\int_0^{\delta} g_{3D}(\sqrt{r_i^2+(z-z_0)^2})\,\mathrm{d}z.$$

Substituting the above expression into (2.2) yields

$$g_{2D}(r_i; z_0, \delta) = \frac{1}{\delta}\int_0^{\delta} g_{3D}(\sqrt{r_i^2+(z-z_0)^2})\,\mathrm{d}z,$$

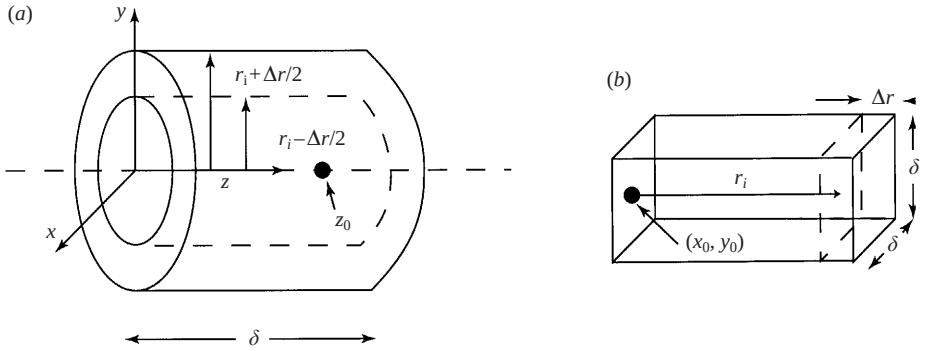


FIGURE 3. Schematic of the control volume of particles sampled around a given particle for (*a*) two-dimensional slice and (*b*) one-dimensional column of particle data.

where we have assumed that the slice volume $A\delta$ is sufficiently large that the expected number of pairs in the slice has converged to the volume average, i.e. $\tilde{P} = PA\delta/V$. This expression is for a specific location of the test particle; however, since all axial locations are equally probable we can average the above uniformly over all $z_0$ to obtain

$$g_{2D}(r_i;\delta) = \frac{1}{\delta^2}\int_0^\delta \int_0^\delta g_{3D}(\sqrt{r_i^2 + (z-z_0)^2})\,\mathrm{d}z\,\mathrm{d}z_0.$$

Finally, the double integral can be reduced to a single integral by recognizing that diagonal lines on the $(z, z_0)$-plane represent constant values of the integrand. Defining $v \equiv (z - z_0)/\delta$ and $\epsilon_i \equiv r_i/\delta$ as the dimensionless separation distance, we arrive at the final expression

$$g_{2D}(\epsilon_i) = 2\int_0^1 (1-v) g_{3D}(\sqrt{\epsilon_i^2 + v^2})\,\mathrm{d}v. \tag{2.4}$$

### 2.2. *One-dimensional relationship*

The development for one-dimensional sampling follows by analogy. The equivalent control volume for the one-dimensional sampling is depicted in figure 3(*b*), where the sample volume of interest is again not $V_i$ but $\hat{V}_i \equiv \delta^2\Delta r$. Following the same procedure outlined above, we obtain

$$g_{1D}(r_i; x_0, y_0, \delta) = \frac{1}{\delta^2}\int_0^\delta \int_0^\delta g_{3D}(\sqrt{r_i^2 + (x-x_0)^2 + (y-y_0)^2})\,\mathrm{d}x\,\mathrm{d}y,$$

where $(x_0, y_0)$ is the location of the test particle. Once again, as all positions on the $(x_0, y_0)$-plane are equally probable, we can average the result uniformly, to give

$$g_{1D}(r_i;\delta) = \frac{1}{\delta^4}\int_0^\delta \int_0^\delta \int_0^\delta \int_0^\delta g_{3D}(\sqrt{r_i^2 + (x-x_0)^2 + (y-y_0)^2})\,\mathrm{d}x\,\mathrm{d}y\,\mathrm{d}x_0\,\mathrm{d}y_0.$$

Making the substitution used earlier in the two-dimensional analysis yields

$$g_{1D}(\epsilon_i) = 4\int_0^1 \int_0^1 (1-v)(1-w) g_{3D}(\sqrt{\epsilon_i^2 + v^2 + w^2})\,\mathrm{d}v\,\mathrm{d}w, \tag{2.5}$$

where $v \equiv (x - x_0)/\delta$, $w \equiv (y - y_0)/\delta$ and again $\epsilon_i \equiv r_i/\delta$. The integration over the $(v, w)$-plane in (2.5) can be reduced further by rewriting it in polar coordinates,

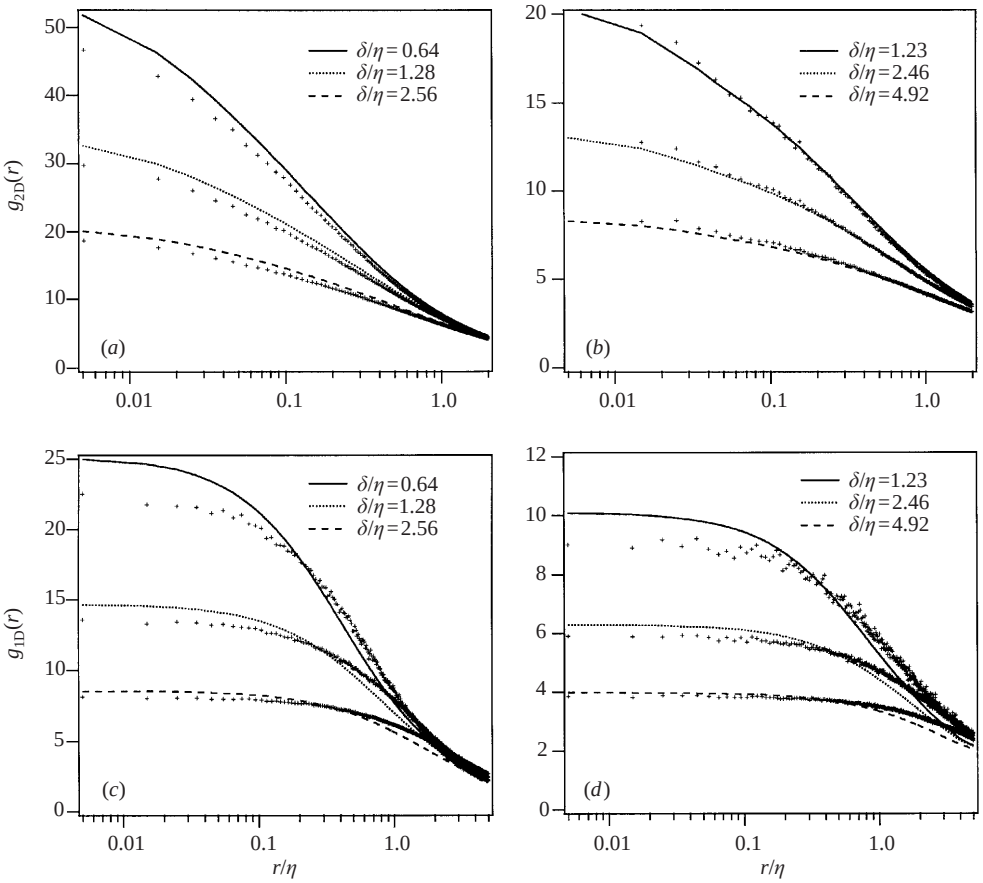


FIGURE 4. Comparison of the prediction for $g_{2D}(r)$ with DNS slice data for (*a*) $St = 0.7$ and (*b*) $St = 0.4$, and the prediction for $g_{1D}(r)$ with DNS column data for (*c*) $St = 0.7$ and (*d*) $St = 0.4$.

replacing $\mathrm{d}v\,\mathrm{d}w$ by $\ell\,\mathrm{d}\theta\,\mathrm{d}\ell$ and performing the integration in $\theta$ analytically

$$g_{1D}(\epsilon_i) = \int_0^{\sqrt{2}} f(\ell) g_{3D}(\sqrt{\epsilon_i{}^2 + \ell^2})\,\ell\,\mathrm{d}\ell, \tag{2.6}$$

where

$$f(\ell) = 4\begin{cases} \frac{1}{2}\pi - 2\ell + \frac{1}{2}\ell^2, & 0 \leqslant \ell \leqslant 1 \\ \frac{1}{2}\pi - 1 - \frac{1}{2}\ell^2 + 2\sqrt{\ell^2 - 1} - 2\tan^{-1}\sqrt{\ell^2 - 1}, & 1 < \ell \leqslant \sqrt{2}. \end{cases}$$

### 2.3. *Comparison with DNS*

The relationships derived in the previous two sections are tested using DNS data corresponding to particle Stokes numbers (defined as the ratio of the particle response time to the Kolmogorov time) of 0.7 and 0.4. Figure 4 shows a comparison between $g_{2D}(r)$ and $g_{1D}(r)$ obtained directly from the DNS with the functions obtained by numerically evaluating the right-hand side of (2.4) and (2.6) using $g_{3D}(r)$ taken from the DNS. The agreement for both $g_{2D}(r)$ and $g_{1D}(r)$ is well within the statistical error of the data, confirming both relationships.

## 3. Inverse relationships

The goal of experiments is to evaluate the three-dimensional RDF; however, because the relationships between it and its lower-dimensional counterparts involve integrals, the inverse problem is not well posed without making assumptions about the form of $g_{3D}(r)$. Previous numerical (Reade & Collins 2000*a*) and theoretical (Balkovsky, Falkovich & Fouxon 2001) works suggest a power law of the form

$$g_{3D}(r) \approx c_0 \left(\frac{\eta}{r}\right)^{c_1}, \tag{3.1}$$

where $c_0$ and $c_1$ are parameters.

### 3.1. *Two-dimensional inverse calculation*

If we substitute (3.1) into (2.4), rearrange and integrate, we obtain

$$g_{2D}(\epsilon) = 2c_0 \left(\frac{\eta}{\delta}\right)^{c_1} \left[\frac{{}_2F_1\left(\frac{1}{2}, \frac{1}{2}c_1, \frac{3}{2}, -1/\epsilon^2\right)}{\epsilon^{c_1}} - \frac{(\epsilon^2)^{1-c_1/2} - (1+\epsilon^2)^{1-c_1/2}}{(c_1-2)}\right], \tag{3.2}$$

where ${}_2F_1(a,b,c,d)$ is the Gauss hypergeometric function (Abramowitz & Stegun 1964). It is useful to consider the asymptotic behaviour of (3.2) for small $r$

$$\lim_{r\to 0} g_{2D} = \tilde{c}_0 \left(\frac{\eta}{r}\right)^{\tilde{c}_1} + \tilde{A} + O\left(\frac{r}{\eta}\right)^2, \tag{3.3}$$

where $\tilde{c}_1 \equiv c_1 - 1$ and $\tilde{c}_0$ and $\tilde{A}$ are coefficients that depend upon $c_0$, $c_1$ and $\delta/\eta$. The result is reminiscent of the so-called 'additive law' for fractals, which states that the dimension of the intersection between a fractal object in three-dimensional space and a two-dimensional plane is one less than the fractal dimension of the original object (see Sreenivasan 1991, p. 545). However, in this case $0 \leqslant c_1 \leqslant 1$ and so $\tilde{c}_1 < 0$, which causes the leading-order terms in the expansion to reverse and $g_{2D} \to \tilde{A}$. Nevertheless, the 'additive law' seems to apply for the RDF as well.

Because the limiting behaviour of $g_{2D}$ is not a simple power law, it is more accurate to regress the coefficients $c_0$ and $c_1$ from (3.2) directly. This can be expressed in terms of a nonlinear minimization of the residual error, $R(c_1)$, defined as

$$R(c_1) \equiv \sum_{i=1}^{M} [g_{2D_i} - c_0 \tilde{g}_{2D}(\epsilon_i)]^2 \quad \text{where} \quad c_0 = \frac{\sum_{i=1}^{M} \tilde{g}_{2D}(\epsilon_i) g_{2D_i}}{\sum_{i=1}^{M} \tilde{g}_{2D}(\epsilon_i)^2}, \tag{3.4}$$

$M$ is the number of experimental points to be regressed, $g_{2D_i}$ is the experimental value at a separation distance $\epsilon_i$, $\tilde{g}_{2D}(\epsilon_i) \equiv g_{2D}(\epsilon_i)/c_0$ is the value obtained from (3.2) without the prefactor $c_0$. Note that because we assume a power law for $g_{3D}(r)$, the curve fit should be done over a range $\epsilon \leqslant \epsilon^*$ that is suitably small such that this assumption is valid.

To test the concept, we used the nonlinear optimization routine `brent.f` from Press *et al.* (1992) to regress $g_{2D}(\epsilon)$ obtained from the two DNS runs shown earlier (see figure 4). A summary of the results is given in table 1. Overall, the percent errors in $c_0$ and $c_1$ are reasonable (e.g. for almost all of the cases the errors are at or below 10%). Notice that the results improve with decreasing $\delta/\eta$ (i.e. decreasing thickness of the slice) as would be expected. The behaviour with $\epsilon^*$ is somewhat more complicated due

| | | $St = 0.7$ | | | | | $St = 0.4$ | | | | |
|---|---|---|---|---|---|---|---|---|---|---|---|
| *Run* | $\epsilon^*$ | $\delta/\eta$ | $c_0$ | *err* | $c_1$ | *err* | $\delta/\eta$ | $c_0$ | *err* | $c_1$ | *err* |
| 1 | 0.2 | 0.64 | 8.28 | 3.27 | 0.735 | 2.26 | 1.23 | 5.43 | 8.43 | 0.758 | 9.22 |
| 2 | 0.5 | 0.64 | 8.08 | 5.61 | 0.745 | 0.931 | 1.23 | 5.60 | 5.56 | 0.741 | 6.77 |
| 3 | 1.0 | 0.64 | 7.94 | 7.24 | 0.753 | 0.133 | 1.23 | 5.69 | 4.05 | 0.730 | 5.19 |
| 4 | 5.0 | 0.64 | 7.77 | 9.23 | 0.765 | 1.73 | 1.23 | 5.92 | 0.169 | 0.694 | 0.00 |
| 5 | 0.2 | 1.28 | 7.65 | 10.6 | 0.777 | 3.32 | 2.45 | 5.77 | 2.70 | 0.750 | 8.07 |
| 6 | 0.5 | 1.28 | 7.77 | 9.23 | 0.768 | 2.13 | 2.45 | 5.87 | 1.01 | 0.732 | 5.48 |
| 7 | 1.0 | 1.28 | 7.76 | 9.35 | 0.769 | 2.26 | 2.45 | 5.94 | 0.169 | 0.717 | 3.31 |
| 8 | 5.0 | 1.28 | 7.75 | 9.46 | 0.769 | 2.26 | 2.45 | 6.07 | 2.36 | 0.656 | 5.48 |
| 9 | 0.2 | 2.56 | 7.64 | 10.7 | 0.784 | 4.26 | 4.90 | 6.12 | 3.20 | 0.618 | 11.0 |
| 10 | 0.5 | 2.56 | 7.72 | 9.81 | 0.773 | 2.79 | 4.90 | 6.01 | 1.35 | 0.650 | 6.34 |
| 11 | 1.0 | 2.56 | 7.73 | 9.70 | 0.771 | 2.53 | 4.90 | 6.01 | 1.35 | 0.654 | 5.76 |
| 12 | 5.0 | 2.56 | 7.80 | 8.88 | 0.755 | 0.399 | 4.90 | 5.81 | 2.02 | 0.573 | 17.4 |

TABLE 1. Values of the coefficients $c_0$ and $c_1$ obtained for the $St = 0.7$ case (left) and $St = 0.4$ case (right) by curve fitting $g_{2D}(\epsilon)$ over the range $\epsilon \leqslant \epsilon^*$. The terms marked *err* show the percentage errors in $c_0$ and $c_1$ compared to the value obtained directly from $g_{3D}(r/\eta)$.

to competing effects. As this parameter decreases, the power-law assumption improves, but the statistical error increases due to the decreasing sample size. Consequently, the trend with $\epsilon^*$ depends on which of these errors is more important. In general, the goal is to reduce $\epsilon^*$ to the point where statistical errors begin to become important.

### 3.2. *One-dimensional inverse calculation*

We can write a similar function for $g_{1D}(\epsilon)$ by substituting (3.1) into (2.5). After expanding the integrand and taking advantage of the symmetries, we obtain

$$g_{1D}(\epsilon) = 4c_0 \left(\frac{\eta}{\delta}\right)^{c_1} [I_1(\epsilon; c_1) - 2I_2(\epsilon; c_1) + I_3(\epsilon; c_1)], \tag{3.5}$$

where

$$I_1(\epsilon; c_1) = \int_0^1 \frac{{}_2F_1\left(\frac{1}{2}, \frac{1}{2}c_1, \frac{3}{2}, -1/(w^2+\epsilon^2)\right)}{(w^2+\epsilon^2)^{c_1/2}}\, \mathrm{d}w, \tag{3.6}$$

$$I_2(\epsilon; c_1) = \frac{1}{2-c_1}[(1+\epsilon^2)^{1-c_1/2}\ {}_2F_1(\tfrac{1}{2}, -1+\tfrac{1}{2}c_1, \tfrac{3}{2}, -1/(1+\epsilon^2)) - \epsilon^{2-c_1}\ {}_2F_1(\tfrac{1}{2}, -1+\tfrac{1}{2}c_1, \tfrac{3}{2}, -1/\epsilon^2)], \tag{3.7}$$

$$I_3(\epsilon; c_1) = \frac{(2+\epsilon^2)^{2-c_1/2} - 2(1+\epsilon^2)^{2-c_1/2} + \epsilon^{4-c_1}}{(2-c_1)(4-c_1)}. \tag{3.8}$$

Note that $I_1(\epsilon; c_1)$ cannot be integrated analytically and therefore was evaluated numerically using Simpson's rule. The asymptotic behaviour of $g_{1D}$ for small $r$ is

$$\lim_{r\to 0} g_{1D} = \hat{c}_0 \left(\frac{\eta}{r}\right)^{\hat{c}_1} + \hat{A}, \tag{3.9}$$

where $\hat{c}_1 \equiv c_1 - 2$, and $\hat{c}_0$ and $\hat{A}$ are coefficients that depend on $c_0$, $c_1$ and $\delta/\eta$. Once again, $\hat{c}_1$ is consistent with the 'additive law' for a three-dimensional fractal, now intersected by a line (Sreenivasan 1991). Furthermore, realistic values for $c_1$ yield $\hat{c}_1 < 0$, causing $g_{1D} \to \hat{A}$ (a constant) in the limit $r \to 0$, as was seen earlier for $g_{2D}$.

| | | $St = 0.7$ | | | | | $St = 0.4$ | | | | |
|---|---|---|---|---|---|---|---|---|---|---|---|
| *Run* | $\epsilon^*$ | $\delta/\eta$ | $c_0$ | *err* | $c_1$ | *err* | $\delta/\eta$ | $c_0$ | *err* | $c_1$ | *err* |
| 1 | 1.0 | 0.64 | 9.70 | 13.3 | 0.601 | 20.1 | 1.23 | 6.40 | 7.93 | 0.484 | 30.3 |
| 2 | 5.0 | 0.64 | 8.54 | 0.234 | 0.773 | 2.79 | 1.23 | 6.25 | 5.40 | 0.560 | 19.3 |
| 3 | 10.0 | 0.64 | 8.33 | 2.69 | 0.752 | 0.00 | 1.23 | 6.25 | 5.40 | 0.564 | 18.7 |
| 4 | 20.0 | 0.64 | 8.29 | 3.15 | 0.758 | 0.798 | 1.23 | 6.23 | 5.06 | 0.548 | 21.0 |
| 5 | 1.0 | 1.28 | 8.92 | 4.21 | 0.589 | 21.7 | 2.45 | 5.84 | 1.52 | 0.479 | 31.0 |
| 6 | 5.0 | 1.28 | 8.53 | 0.350 | 0.713 | 5.19 | 2.45 | 5.93 | 0.00 | 0.520 | 25.1 |
| 7 | 10.0 | 1.28 | 8.53 | 0.350 | 0.733 | 2.53 | 2.45 | 5.89 | 0.675 | 0.510 | 26.5 |
| 8 | 20.0 | 1.28 | 8.53 | 0.350 | 0.726 | 3.46 | 2.45 | 5.70 | 3.88 | 0.478 | 31.1 |
| 9 | 1.0 | 2.56 | 8.02 | 6.31 | 0.578 | 23.1 | 4.90 | 5.18 | 12.6 | 0.439 | 36.7 |
| 10 | 5.0 | 2.56 | 8.28 | 3.27 | 0.680 | 9.57 | 4.90 | 5.26 | 11.3 | 0.456 | 34.3 |
| 11 | 10.0 | 2.56 | 8.27 | 3.39 | 0.679 | 9.71 | 4.90 | 5.03 | 15.2 | 0.428 | 38.3 |
| 12 | 20.0 | 2.56 | 8.06 | 5.84 | 0.645 | 14.2 | 4.90 | 4.63 | 21.9 | 0.383 | 44.8 |

TABLE 2. Values of the coefficients $c_0$ and $c_1$ obtained for the $St = 0.7$ case (left) and $St = 0.4$ case (right) by curve fitting $g_{1D}(r/\eta)$ at values of $r/\delta$ below $\epsilon^*$. The terms marked *err* show the percentage errors in $c_0$ and $c_1$ compared to the value obtained directly from $g_{3D}(r/\eta)$.

We applied the same regression procedure to the $g_{1D}(\epsilon)$ data obtained from DNS. Table 2 shows a summary of the results for $St = 0.7$ and $St = 0.4$. Notice that we increased the range of $\epsilon^*$ relative to the two-dimensional case. This was done to reduce (somewhat) the errors in the regressed values of $c_0$ and $c_1$. However, despite the adjustment, the errors are found to be considerably larger than for the two-dimensional regression. Some insight into the origin of the problem can be found by considering $g_{1D}(r/\eta)$ shown in figure 2(*a*). At small $r/\eta$ (corresponding to small $\epsilon$ in the regression analysis), the slope is more shallow than for the two-dimensional RDF. Consequently, the regression of the parameters $c_0$ and $c_1$ is more susceptible to statistical errors in the distribution. This can be seen by comparing the errors in the $St = 0.7$ and $St = 0.4$ data. In both analyses, the error in the $St = 0.4$ data was greater than for the $St = 0.7$ data; however, the adverse effect of this error on the estimate for $c_1$ was substantially greater for the one-dimensional analysis than for the two-dimensional analysis (see for example the *err* column for $c_1$ in tables 1 and 2 under $St = 0.4$).

The problem appears to be inherent to the 1D RDF, which by definition has lost information along two axes of the measurement (instead of one). The lost information causes $g_{1D}(\epsilon)$ to be relatively flat over the range of $\epsilon$ where the power-law assumption applies. This can only be mitigated to some extent by minimizing the statistical error of the data (i.e. increasing the data size).

## 4. Conclusions

In this paper, we derived relationships between the three-dimensional RDF and the two- and one-dimensional functions obtained from lower-dimensional sampling of the data. Lower-dimensional RDFs were attenuated at separations below the characteristic length of the measurement (defined as $\delta$ in our nomenclature). Forward relationships for $g_{2D}$ and $g_{1D}$ were derived exactly in terms of weighted integrals of $g_{3D}$ (see (2.4) and (2.6)). It must be emphasized that these relationships only assume that the particle field is *isotropic*, but are otherwise general. In contrast, the inverse

relationships for $g_{3D}$ in terms of $g_{2D}$ or $g_{1D}$ are not well posed without assuming a functional form for $g_{3D}$. Here, we showed the inverse relationships assuming a power-law – a good approximation for aerosol particles in turbulence. We observed that the exponent for the 'leading-order' term for $g_{2D}$ and $g_{1D}$ obeyed the so-called additive law; however, this could not be fully exploited because realistic values for $c_1$ caused a re-ordering of the terms that disrupted the power-law behaviour for $g_{2D}$ and $g_{1D}$. We therefore proposed an alternative algorithm to regress $c_0$ and $c_1$ based on the full expressions for $g_{2D}$ and $g_{1D}$ (see (3.2) and (3.5) and related discussion).

The results of this study have important implications for interpreting experimental measurements of droplet clustering, including measurements made in clouds. Even neglecting the errors associated with the measurement (see the discussion of errors in Kostinski & Shaw 2001), we have shown that the RDF obtained directly from the data is much smaller than the three-dimensional RDF. The debate about the importance of droplet clustering in the evolution of clouds would therefore benefit from an analysis of the data that takes advantage of (3.5) to obtain an approximation for the intrinsic function $g_{3D}(r)$.

This work was supported by the NASA microgravity fluids physics program.

## REFERENCES

Abramowitz, M. & Stegun, I. A. 1964 *Handbook of Mathematical Functions*. Dover.

Baker, B. A. 1992 Turbulent entrainment and mixing in clouds: A new observational approach. *J. Atmos. Sci.* **49**, 387–404.

Balkovsky, E., Falkovich, G. & Fouxon, A. 2001 Intermittent distribution of inertial particles in turbulent flows. *Phys. Rev. Lett.* **86**, 2790–2793.

Brenguier, J.-L., Bourrianne, T., Coelho, A. A., Isbert, J., Peytavi, R., Trevarin, D. & Wechsler, P. 1998 Improvements of the droplet size distribution measurements with the Fast-FSSP. *J. Atmos. Oceanic Technol.* **15**, 1077–1090.

Chaumat, L. & Brenguier, J.-L. 2001 Droplet spectra broadening in cumulus clouds. Part II: Microscale droplet concentration heterogeneities. *J. Atmos. Sci.* **58**, 642–654.

Kostinski, A. B. & Shaw, R. A. 2001 Scale-dependent droplet clustering in turbulent clouds. *J. Fluid Mech.* **434**, 389–398.

Lei, X., Ackerson, B. J. & Tong, P. 2001 Settling statistics of hard sphere particles. *Phys. Rev. Lett.* **86**, 3300–3303.

McQuarrie, D. A. 1976 *Statistical Mechanics*. Harper & Row.

Press, W. H., Teukolsky, S. A., Vetterling, W. T. & Flannery, B. P. 1992 *Numerical Recipes*. Cambridge University Press.

Pu, Y. & Meng, H. 2000 An advanced off-axis holographic particle image velocimetry (hpiv) system. *Exps. Fluids* **29**, 184–197.

Reade, W. C. & Collins, L. R. 2000*a* Effect of preferential concentration on turbulent collision rates. *Phys. Fluids* **12**, 2530–2540.

Reade, W. C. & Collins, L. R. 2000*b* A numerical study of the particle size distribution of an aerosol undergoing turbulent coagulation. *J. Fluid Mech.* **415**, 45–64.

Squires, K. D. & Eaton, J. K. 1991 Preferential concentration of particles by turbulence. *Phys. Fluids A* **3**, 1169.

Sreenivasan, K. R. 1991 Fractals and multifractals in fluid turbulence. *Annu. Rev. Fluid Mech.* **23**, 539–600.

Sundaram, S. & Collins, L. R. 1997 Collision statistics in an isotropic, particle-laden turbulent suspension I, direct numerical simulations. *J. Fluid Mech.* **335**, 75–109.

Wang, L. P. & Maxey, M. R. 1993 Settling velocity and concentration distribution of heavy particles in homogeneous isotropic turbulence. *J. Fluid Mech.* **256**, 27.

Wang, L.-P., Wexler, A. S. & Zhou, Y. 2000 Statistical mechanical description and modeling of turbulent collision of inertial particles. *J. Fluid Mech.* **415**, 117–153.

Zhang, J., Tao, B. & Katz, J. 1997 Turbulent flow measurement in a square duct with hybrid holographic PIV. *Exps. Fluids* **23**, 373–381.